

# Efficient Evaluation of Nonlocal Pseudopotentials via Euler Exponential Spline Interpolation

Hee-Seung Lee,<sup>[b]</sup> Mark E. Tuckerman,<sup>\*,[a]</sup> and Glenn J. Martyna<sup>[c]</sup>

An Euler exponential spline (EES) based formalism is employed to derive new expressions for the electron–atom nonlocal pseudopotential interaction (NL) in electronic structure calculations performed using a plane wave basis set that can be computed more rapidly than standard techniques. Two methods, one that is evaluated by switching between real and reciprocal space via fast Fourier transforms, and another that is evaluated completely in real space, are described. The reciprocal-space or *g*-space-based technique, NLEES-G, scales as  $NM\log M \sim N^2\log N$ , where  $N$  is the number of electronic orbitals and  $M$  is the number of plane waves. The real-space based technique, NLEES-R, scales as  $N^2$ . The latter can potentially be used within a maximally spatially localized orbital method to yield linear scaling, while the former

could be employed within a maximally delocalized orbital method to yield  $N\log N$  scaling. This behavior is to be contrasted with standard techniques, which scale as  $N^3$ . The two new approaches are validated using several examples, including solid silicon and liquid water, and demonstrated to be improvements on other, reduced-order nonlocal techniques. Indeed, the new methods have a low overhead and become more efficient than the standard technique for systems with roughly 20 or more atoms. Both NLEES methods are shown to work stably and efficiently within the Car–Parrinello *ab initio* molecular dynamics framework, owing to the existence of  $p-2$  continuous derivatives of a  $p$ th-order spline.

## 1. Introduction

*Ab initio* molecular dynamics (AIMD) has emerged as a powerful theoretical technique for studying complex chemical phenomena. AIMD allows chemical bond-breaking and forming events to be treated in a natural way by combining finite-temperature molecular dynamics with electronic-structure calculations performed “on the fly” to generate the interatomic forces. The AIMD methodology has been successfully applied to a wide variety of important problems in chemistry, physics, and biology.<sup>[1–3]</sup>

Despite AIMD’s success, the computational overhead associated with the calculations is substantial. The most commonly employed implementation of AIMD is based on the Car–Parrinello approach,<sup>[4]</sup> wherein the electronic structure is represented within the Kohn–Sham (KS) formulation of density functional theory (DFT), the KS orbitals are expanded in a plane-wave basis, and a fictitious adiabatic dynamics is used to generate, approximately, the minimum of the KS energy functional at each nuclear configuration. In a plane wave basis, in particular, explicit treatment of core electronic orbitals is computationally intractable, and, hence, these orbitals are typically replaced by electron–atom nonlocal pseudopotentials. However, the computation of nonlocal pseudopotential interactions scales as  $N^2M$ , where  $N$  is the number of remaining valence KS orbitals and  $M$  is the number of plane waves, the same scaling as the orbital orthogonality requirement. Since  $M$  scales as  $N$ , this leads to the well-known  $N^3$  computational cost of plane-wave-based DFT methods.

Herein, an Euler exponential spline (EES)<sup>[5,6]</sup> based formalism is developed for nonlocal (NL) pseudopotentials that reduces the scaling of the calculation of the nonlocal energies, atomic

forces, and gradients with respect to plane wave expansion coefficients. The Euler exponential spline formalism has been employed to reduce the scaling with system size of Ewald summation for point charges under a three-dimensional periodic boundary conditions<sup>[7]</sup> as well as in clusters, wires, and surfaces.<sup>[8–10]</sup> It has also been employed to treat permanent and induced dipole interactions.<sup>[11]</sup> Here, an Euler exponential spline interpolation of the atomic structure factor in the electron–atom pseudopotentials leads to two possible schemes: a reciprocal-space or *g*-space based scheme that scales as  $NM\log M \sim N^2 \sim N^2\log N$  and a real-space based approach that scales as  $N^2$ . The latter technique can be made to scale as  $N$  (linearly) for spatially localized orbitals while the former can be made to scale as  $M\log N$  for spatially delocalized orbitals.<sup>[12]</sup> Recently, a new quantum field theoretic approach was introduced for propagating such maximally localized (Wannier functions) or delocalized orbitals within the Car–Parrinello framework,<sup>[13–15]</sup> and it is expected that the present method will figure prominently in such a scheme with the aim of producing a novel

[a] Prof. M. E. Tuckerman  
Department of Chemistry and Courant Institute of Mathematical Sciences  
New York University, New York NY 10003 (USA)  
Fax: (1) 212-260-7905  
E-mail: mark.tuckerman@nyu.edu

[b] Dr. H.-S. Lee  
Department of Chemistry  
New York University, New York NY 10003 (USA)

[c] Dr. G. J. Martyna  
Physical Sciences Division  
IBM TJ Watson Research Center, Yorktown Heights, NY 10598 (USA)

linear scaling AIMD approach. The Euler exponential spline based methods are continuously differentiable and have a low computational overhead, which allows them to replace standard methods for systems of approximately twenty atoms or more and can be used stably within the Car–Parrinello approach. They, therefore, constitute a substantial advance over existing schemes for reducing the scaling of the calculation of nonlocal pseudopotentials.<sup>[16–18]</sup>

Although the formulation presented herein focuses on the Kleinman–Bylander projector form of the nonlocal pseudopotential,<sup>[19]</sup> the ideas discussed carry over to other types of pseudopotentials, including ultrasoft pseudopotentials,<sup>[20]</sup> semilocal forms handled via Gauss–Hermite integration, and the recently introduced Goedecker–Hutter form.<sup>[21,22]</sup> Note, in addition, the present methodology can be employed in conjunction with localized basis sets, such as Gaussians<sup>[23]</sup> and discrete variable representations,<sup>[24,25]</sup> which, also, could benefit from the reduction in basis set size made possible by the replacement of core electrons with nonlocal pseudopotentials.

This Article is organized as follows: In Section 2, the Euler exponential spline  $\mathbf{g}$ -space (NLEES-G) and real-space (NLEES-R) methods for treating nonlocal pseudopotentials will be developed. Both the energy and its derivative with respect to atom positions and orbital expansion coefficients will be discussed. In Section 3, several example systems will be presented to illustrate the power of the new approach. Finally, conclusions will be given in Section 4.

## 2. Methodology

In the Car–Parrinello AIMD scheme, the electrons are represented by a set of orbitals,  $\{\psi_i(\mathbf{r})\}$ , which closely follow the atom dynamics and remain on the instantaneous Born–Oppenheimer ground-state surface. This is accomplished by introducing fictitious dynamics of orbitals into the system Lagrangian, which can be written for the full system (that is, atom plus fictitious dynamics) as Equation (1):

$$L = \mu \sum_i \langle \dot{\psi}_i | \dot{\psi}_i \rangle + \frac{1}{2} \sum_l M_l \dot{\mathbf{R}}_l^2 - E[\{\psi_i\}, \{\mathbf{R}_l\}] + \sum_{ij} \lambda_{ij} (\langle \psi_i | \psi_j \rangle - \delta_{ij}) \quad (1)$$

where  $\mu$  is the mass associated with the fictitious orbital dynamics,  $M_l$  and  $\mathbf{R}_l$  are the mass and the position of atom  $l$ , and  $\{\lambda_{ij}\}$  is a set of Lagrange multipliers that impose the orthonormality of orbitals. Within the Kohn–Sham DFT, the energy functional is given by Equation (2):

$$E[\{\psi_i\}, \{\mathbf{R}_l\}] = T_s[\{\psi_i\}] + E_H[n] + E_{xc}[n] + E_N[\{\mathbf{R}_l\}] + E_{\text{ext}}[n; \{\mathbf{R}_l\}] \quad (2)$$

where  $n(\mathbf{r}) = \sum_i f_i |\psi_i(\mathbf{r})|^2$  is the electron density,  $f_i$  is the occupation number of the  $i$ th orbital,  $T_s$  is the kinetic energy of Kohn–Sham non-interacting electron system,  $E_H$  is the Hartree

energy,  $E_{xc}$  is the exchange–correlation energy, and  $E_N$  is the electrostatic interaction between atoms.

The last term in Equation (2),  $E_{\text{ext}}$ , represents the interaction between electrons and atoms. When a plane wave basis set is employed to expand orbitals, the core electrons are typically replaced by nonlocal atomic pseudopotentials. This is accomplished by introducing an effective potential that contains a different radial potential for each angular momentum channel of each atom, Equation (3):

$$\hat{V}_{\text{pseud}} = \sum_J \sum_{l(J)} \sum_{l=0}^{\infty} \sum_{m=-l}^l v_J^{(l)}(r_{l(J)}) |lm\rangle \langle lm| \quad (3)$$

In Equation (3),  $l(J)$  is a restricted index that runs only over the atoms of type  $J$ , such that  $\sum_J \sum_{l(J)} = N$ , the number of atoms in the system,  $r_{l(J)}$  is the radial distance from the electron to atom  $l(J)$ ,  $v_J^{(l)}(r)$  is the  $l$ -channel radial pseudopotential for atom type  $J$ , and  $|lm\rangle \langle lm|$  is a projection operator onto angular momentum eigenstate,  $|lm\rangle$ . The external energy, computed according to  $E_{\text{ext}} = \sum_i \langle \psi_i | \hat{V}_{\text{pseud}} | \psi_i \rangle$ , clearly takes on a nonlocal character, involving two angular integrals and a single radial integral ( $d\Omega d\Omega' r^2 dr$ ). A further approximation involves retaining the angular momentum dependence only up to a maximum value  $\bar{l}-1$ , achieved by adding and subtracting  $v_J^{(\bar{l})}(r)$  in Equation (3) and truncating the sum at  $\bar{l}-1$ . As a consequence of the latter approximation, the pseudopotential is decomposed into two terms, a local term,  $E_{\text{loc}}[n, \{\mathbf{R}\}]$ , that grossly treats the higher angular momentum components and a nonlocal term,  $E_{\text{NL}}[\{\psi\}, \{\mathbf{R}\}]$ , that both depends explicitly on angular momentum channels with  $l$  less than or equal to  $\bar{l}-1$  and directly on the orbitals rather than on the density. It was shown by Kleinman and Bylander<sup>[19]</sup> that the nonlocal term can be written in a fully separable form (integrating over  $d\mathbf{r} d\mathbf{r}'$ ) for a wide range of elements provided appropriate care is taken,<sup>[26]</sup> thereby reducing the computational overhead over the more exact semilocal form.

A plane wave basis set allows many of terms in the density functional to be computed in their diagonal representation. This is accomplished by switching between the real-space and  $\mathbf{g}$ -space representation of the orbitals and the density using three-dimensional fast Fourier transforms (3DFFT). In fact, if the pseudopotentials are purely local, each term in the energy functional can be computed with a scaling better than  $NM \log M \sim N^2 \log N$ , where  $N$  is the number of orbitals and  $M$  is the number of plane waves (although the orthogonalization of the orbitals still scales as  $N^2 M \sim N^3$ ). In the proceeding sections, the reciprocal-space and real-space formalisms for improving the scaling of the nonlocal pseudopotential calculation are described.

### 2.1. Nonlocal Pseudopotential Calculation

The determination of the nonlocal energy and forces scales as  $N^2 M$  and is the most computationally intensive term in the electron–atom interaction. In the fully separable Kleinman and Bylander (KB) form, the nonlocal part of  $E_{\text{ext}}$  is given by Equa-

tions (4) and (5):

$$E_{\text{NL}} = \sum_i f_i \sum_J \sum_{l(J)} \int d\mathbf{r} d\mathbf{r}' \psi_i^*(\mathbf{r}') \psi_i(\mathbf{r}) \left[ \sum_{l=0}^{\bar{l}-1} \sum_{m=-l}^{m=l} C_{Jl} F_{Jlm}^*(\mathbf{r} - \mathbf{R}_{l(J)}) F_{Jlm}(\mathbf{r}' - \mathbf{R}_{l(J)}) \right] \quad (4)$$

$$= \sum_i f_i \sum_J \sum_{l(J)} \sum_{l=0}^{\bar{l}-1} \sum_{m=-l}^{m=l} C_{Jl} Z_{il(J)l}^* Z_{il(J)l} \quad (5)$$

where  $F_{Jlm}(\mathbf{r})$  is an appropriate set of angular momentum,  $l$  and  $m$  and atom type,  $J$ , dependent functions,  $C_{Jl}$  is a weight factor, and the quantity  $Z_{il(J)l}$  is defined by Equation (6):

$$Z_{il(J)l} = \int d\mathbf{r} F_{Jlm}(\mathbf{r} - \mathbf{R}_{l(J)}) \psi_i(\mathbf{r}) \quad (6)$$

When the orbitals are expanded in a plane wave basis at the  $\Gamma$ -point of the Brillouin zone according to  $\psi_i(\mathbf{r}) = (1/\sqrt{V}) \sum_{\mathbf{g}} \bar{\psi}_i(\mathbf{g}) \exp(i\mathbf{g} \cdot \mathbf{r})$ , then  $Z_{il(J)l}$  can be evaluated in  $\mathbf{g}$ -space, Equation (7):

$$Z_{il(J)l} = \frac{1}{\sqrt{V}} \sum_{\mathbf{g}} \tilde{F}_{Jlm}(\mathbf{g}) \bar{\psi}_i(\mathbf{g}) e^{i\mathbf{g} \cdot \mathbf{R}_{l(J)}} \quad (7)$$

where the  $\bar{\psi}_i(\mathbf{g})$  are a set of Fourier series coefficients,  $V = \text{deth} \mathbf{h}$  is the volume of the simulation cell,  $\mathbf{h}$  is the matrix whose rows contain the Cartesian coordinates of the  $\mathbf{a}, \mathbf{b}, \mathbf{c}$  axes that define the simulation cell/parallelepiped,  $\mathbf{g} = 2\pi \mathbf{h}^{-1} \hat{\mathbf{g}}$  with  $\hat{\mathbf{g}}$  a vector of integers, and  $\tilde{F}_{Jlm}(\mathbf{g})$  is the Fourier transform of  $F_{Jlm}(\mathbf{r})$ , Equation (8):

$$\tilde{F}_{Jlm}(\mathbf{g}) = 4\pi Y_{lm}(\theta_{\mathbf{g}}, \phi_{\mathbf{g}}) \int_0^{\infty} dr r^2 j_R(gr) \Delta v_J^{(l)}(r) \phi_{Jl}^{(0)}(r) \quad (8)$$

Here,  $j_l(r)$  is a spherical Bessel function,  $Y_{lm}(\theta, \phi)$  is a spherical harmonic,  $\Delta v_J^{(l)}(r) = v_J^{(l)}(r) - v_J^{(\bar{l})}(r)$  is the difference between the  $l$  and  $\bar{l}$  angular momentum channel potential functions and  $\phi_{Jl}^{(0)}(r)$  is the ground-state,  $l$ -channel, radial eigenfunction. It is evident from Equations (5) and (7) that the evaluation of the nonlocal energy and force scales as  $NN_p M$ , where  $N_p$  is the number of atoms. Since  $N$  and  $M$  increase as  $N_p$  increases at fixed density, the computational cost of the nonlocal pseudopotential calculation scales effectively as  $N^3$ .

## 2.2. Reduced-Order $\mathbf{g}$ -Space Formalism: NLESS-G

In this subsection, a  $\mathbf{g}$ -space-based approach is presented which achieves  $NM \log M$  scaling for the nonlocal pseudopotential calculation. A plane-wave expansion of orbitals is employed which is truncated on the basis of an energy cutoff,  $E_{\text{cut}} = \hbar^2 g_{\text{max}}^2 / 2m_e$ , and the matrix element,  $Z_{il(J)l}$ , of Equation (7) is recast using the Euler exponential spline.<sup>[5,6]</sup> Specifically, Euler exponential spline interpolation is introduced for

the atomic structure factor,  $\exp(i\mathbf{g} \cdot \mathbf{R}_{l(J)})$ <sup>[7-10]</sup> which permits the nonlocal energy to be evaluated via three-dimensional fast Fourier transforms (3DFFT), thereby reducing the scaling from  $N^3$  to  $NM \log M$ .

To apply the Euler exponential spline interpolation scheme to the atomic structure factor, scaled fractional coordinates  $\mathbf{u}_{l(J)}$  are defined  $u_{l(J),\alpha} = N_{\alpha} \mathbf{h}_{\alpha}^{-1} \cdot \mathbf{R}_{l(J)}$   $\alpha = a, b, c$ , where  $\mathbf{h}_{\alpha}$  is the column of  $\mathbf{h}^{-1}$  corresponding to the  $\alpha$  direction of the cell and  $N_{\alpha}$  is the number of nodes in the spline along the  $\alpha$  direction. The structure factor is then approximated by Equations (9) and (10):

$$e^{i\mathbf{g} \cdot \mathbf{R}_{l(J)}} = \prod_{\alpha=a,b,c} e^{2\pi i \hat{g}_{\alpha} u_{l(J),\alpha} / N_{\alpha}} \quad (9)$$

$$e^{2\pi i \hat{g}_{\alpha} u_{l(J),\alpha} / N_{\alpha}} \approx d_p(\hat{g}_{\alpha}, N_{\alpha}) \sum_{\hat{s}_{\alpha}=-\infty}^{\infty} M_p(u_{l(J),\alpha} - \hat{s}_{\alpha}) e^{2\pi i \hat{g}_{\alpha} \hat{s}_{\alpha} / N_{\alpha}} \quad (10)$$

where  $\hat{g}_{\alpha}$  and  $\hat{s}_{\alpha}$  are integers,  $p-1$  is the spline order, and  $N_{\alpha}$  defines a discrete real space. The spline weight,  $d_p(\hat{g}_{\alpha}, N_{\alpha})$ , is given by Equation (11):

$$d_p(\hat{g}_{\alpha}, N_{\alpha}) = e^{2\pi i (p-1) \hat{g}_{\alpha} / N_{\alpha}} \left[ \sum_{k=0}^{p-2} M_p(k+1) e^{2\pi i \hat{g}_{\alpha} k / N_{\alpha}} \right]^{-1} \quad (11)$$

Like all splines, the Euler spline is exact at the knots, for example, when  $\mathbf{u}_{l(J)}$  is an integer/falls on a grid point. Although the sum over  $\hat{s}_{\alpha}$  covers all the integers in Equation (10), in practice, it becomes finite owing to the finite support of Cardinal B-splines,  $M_p(u)$ , Equation (12):

$$\begin{aligned} M_2(u) &= 1 - |u-1|, \quad 0 \leq u \leq 2 \\ M_2(u) &= 0, \quad u < 0, \quad u > 2 \\ M_p(u) &= \left(\frac{u}{p-1}\right) M_{p-1}(u) + \left(\frac{p-u}{p-1}\right) M_{p-1}(u-1), \quad p > 2 \end{aligned} \quad (12)$$

One of the important properties of Cardinal B-splines is that they are  $p-2$  times continuously differentiable for  $p > 2$ . The derivatives satisfy the recursion relation, Equation (13):

$$\frac{d}{du} M_p(u) = M_{p-1}(u) - M_{p-1}(u-1) \quad (13)$$

which simplifies computation of the force on the atoms. The error associated with exponential spline approximation to the structure factor is given by  $(2|\hat{g}_{\alpha}|/N_{\alpha})^p$ . Hence,  $N_{\alpha}$  must be selected strictly greater than the largest reciprocal lattice vector allowed by the plane-wave cutoff on the orbitals in the  $\alpha$  direction,  $N_{\alpha}^{(\text{orb})}$ . Given  $N_{\alpha} > N_{\alpha}^{(\text{orb})}$  and  $p > 2$ , these two parameters can be adjusted to control accuracy and optimize efficiency. Note that the discrete real space required here is smaller than that required to compute the electron density,  $N_{\alpha}^{(\text{dens})} = 2N_{\alpha}^{(\text{orb})}$ .

Inserting Equation (10) into Equation (7) yields the  $\mathbf{g}$ -space representation of  $Z_{il(J)l}$ , Equation (14):

$$Z_{i(l)Jlm} = \frac{1}{\sqrt{V}} \sum_{\mathbf{s}} \left[ \prod_{\alpha=a,b,c} M_p(u_{l(\alpha),\alpha} - \hat{s}_\alpha) \right] P_{iJlm}(\hat{\mathbf{s}}) \quad (14)$$

where  $P_{iJlm}(\mathbf{s})$  and  $P_{iJlm}(\mathbf{g})$  are given by Equation (15):

$$P_{iJlm}(\mathbf{s}) = \sum_{\mathbf{g}} \bar{P}_{iJlm}(\mathbf{g}) e^{2\pi i \mathbf{g} \cdot \mathbf{s}}$$

$$\bar{P}_{iJlm}(\mathbf{g}) = \left[ \prod_{\alpha=a,b,c} d_p(\hat{\mathbf{g}}_\alpha, N_\alpha) \right] \bar{\psi}_i(\mathbf{g}) \tilde{F}_{Jlm}(\mathbf{g}) \quad (15)$$

and  $\mathbf{s} = (\hat{s}_a/N_a, \hat{s}_b/N_b, \hat{s}_c/N_c)$ . The quantity  $P_{iJlm}(\mathbf{s})$  is defined on a discrete  $N_a \times N_b \times N_c$  real-space grid, and the summation over  $\mathbf{g}$  can, therefore, be performed efficiently by an  $N_a \times N_b \times N_c$  3DFFT. Since  $P_{iJlm}(\mathbf{s})$  depends only on atom type through  $\tilde{F}_{Jlm}(\mathbf{g})$ , the full set of  $P_{iJlm}(\mathbf{s})$  is obtained by performing a 3DFFT for each orbital, angular momentum channel, and atom type present. Both the number of orbitals and the number of plane waves increase linearly with the system size, and the 3DFFT scales as  $M \log M$ . Therefore, computing the full set of  $P_{iJlm}(\mathbf{s})$  scales as  $NM \log M$ . Once a given  $P_{iJlm}(\mathbf{s})$  has been computed, the summation over the discrete grid is performed to obtain  $Z_{i(l)Jlm}$ . Now, the Cardinal B-splines are nonzero only at the  $p$  grid points in each direction, the sum over the discrete real-space grid in Equation (14) is a  $p^3$  operation that does not depend on the system size. Since  $Z_{i(l)Jlm}$  must be evaluated for each orbital and atom, computing all the  $Z_{i(l)Jlm}$  from  $P_{iJlm}(\mathbf{s})$  scales as  $p^3 N^2$ . Consequently, the computation of the nonlocal energy is dominated by the cost of evaluating the  $P_{iJlm}(\mathbf{s})$ .

To determine the force on each atom, the derivative of  $Z_{i(l)Jlm}$  with respect to the atom position is required. Since only the Cardinal B-splines depend on the atom positions in Equation (14), the derivative is obtained by employing the chain rule with Equation (13). As noted earlier, Cardinal B-splines are continuously differentiable and the atomic forces are, therefore, well-behaved. The procedure to compute the forces is, thus, nearly identical to that employed to compute the energy.

The orbital gradients for use in the Car–Parrinello evolution or energy minimization can also be evaluated in an efficient manner. As above, it is useful to exploit the fact that there is a finite number of atom types, Equation (16):

$$\frac{\partial E_{\text{NL}}}{\partial \psi_i^*(\mathbf{g})} = f_i \sum_J \sum_{l(J)} \sum_I \sum_m C_{Jl} \frac{\partial Z_{i(l)Jlm}^*}{\partial \psi_i^*(\mathbf{g})} Z_{i(l)Jlm}$$

$$= \frac{f_i}{\sqrt{V}} \left[ \prod_{\alpha=a,b,c} d_p^*(\hat{\mathbf{g}}_\alpha, N_\alpha) \right] \sum_{lm} \sum_J C_{Jl} \tilde{F}_{Jlm}^*(\mathbf{g}) \bar{Q}_{iJlm}(\mathbf{g}) \quad (16)$$

where  $\bar{Q}_{iJlm}(\mathbf{g})$  and  $Q_{iJlm}(\mathbf{s})$  are given by Equation (17):

$$\bar{Q}_{iJlm}(\mathbf{g}) = \sum_{\mathbf{s}} Q_{iJlm}(\mathbf{s}) e^{-2\pi i \mathbf{g} \cdot \mathbf{s}}$$

$$Q_{iJlm}(\mathbf{s}) = \sum_{l(J)} \left[ \prod_{\alpha=a,b,c} M_p(u_{l(\alpha),\alpha} - \hat{s}_\alpha) \right] Z_{i(l)Jlm} \quad (17)$$

Therefore, the  $\bar{Q}_{iJlm}(\mathbf{g})$  can be created using the same number of 3DFFTs required to create the  $P_{iJlm}$ . Since the number of atom types is a small number that is independent of the system size, the cost of computing the orbital gradients scales as  $NM \log M$ .

The NLEES-G algorithm is summarized briefly:

1. At the start of the calculation, loop over angular momentum and atom types ( $Jlm$ ): compute  $\tilde{F}_{Jlm}(\mathbf{g})$ . These are calculated once and stored for the duration of the simulation.
2. Loop over the orbitals ( $i$ ): compute  $\bar{P}_{iJlm}(\mathbf{g})$  and perform a 3DFFT to yield  $P_{iJlm}(\mathbf{s})$ . Set  $Q_{iJlm}(\mathbf{s}) = 0$ .
3. Loop over the atoms,  $l$ , of type,  $J$  or  $l(J)$ . i) Loop over  $\hat{s}_{\alpha,j}$ ,  $\alpha = 1, 3$ ,  $j = 1, p$ : compute  $Z_{i(l)Jlm}$  by summing over the  $p^3$  nonzero points in real space and increment the nonlocal energy. ii) In addition, increment  $Q_{iJlm}(\hat{\mathbf{s}})$  and compute the force on atom,  $l(J)$ .
4. End loop over atoms  $l$  of type  $J$ .
5. Perform a 3DFFT to compute  $\bar{Q}_{iJlm}(\mathbf{g})$ . Compute the gradient with respect to orbital,  $i$ .
6. End loops over orbitals, angular momentum and atom types.

Note, the required  $\mathbf{g}$ -space is a sphere of radius  $\propto E_{\text{cut}}^{1/2} < N_\alpha/2$  which can be used to reduce the computational cost of evaluating the  $N_a \times N_b \times N_c$  3DFFTs considerably. The algorithmic procedure shown above makes clear the fact that  $\bar{P}_{iJlm}(\mathbf{g})$  needs to be computed for each nonlocal atom type. Consequently, NLEES-G will scale linearly with the number of nonlocal atom types.

### 2.3. Reduced-Order Real Space Formalism: NLEES-R

In this subsection, a new real-space-based approach to the nonlocal pseudopotential calculation, capable of achieving  $N^2$  scaling, is described. The derivation begins by determining two length scales, a small (Cartesian) length scale,  $\Delta$ , below which the nonlocal pseudopotential projector,  $F_{Jlm}(\mathbf{r}) = Y_{lm}(\Omega) \Delta v_{Jl}(r) \phi_{Jl}^{(0)}(r)$  can be assumed to be slowly varying and a large length scale,  $r_{\text{cut}}$  beyond which the projector can be assumed to vanish. Using these two assumptions and further assuming the simulation cell encompasses the large length scale, it is possible to evaluate the nonlocal matrix element using trapezoidal rule integration in the fractional coordinates of the cell,  $\mathbf{r} = \mathbf{h}\mathbf{s}$ ,  $\mathbf{s} = \mathbf{h}^{-1}\mathbf{r}$ ,  $d\mathbf{r} = V d\mathbf{s}$ , Equation (18):

$$Z_{i(l)Jlm} = \left[ \frac{V}{\prod_\alpha N_\alpha} \right] \sum_{\mathbf{s}} F_{Jlm}(\mathbf{h}\mathbf{s} - \mathbf{R}_{l(J)}) \psi_i(\mathbf{h}\mathbf{s}) \quad (18)$$

where the grid spacing is  $\Delta_{s_\alpha} = N_\alpha^{-1}$ ,  $s_\alpha = \hat{s}_\alpha/N_\alpha$ , and the prime indicates that the sum is restricted to  $|\mathbf{h}\mathbf{s} - \mathbf{R}_{l(J)}| < r_{\text{cut}}$ . Using  $N_\alpha = N_\alpha^{(\text{dens})}$  ensures that if the projector can be expressed as a Fourier series with  $|\mathbf{g}| < E_{\text{cut}}$  and  $\mathbf{R}_{l(J)}$  lies on a grid point,  $\mathbf{R}_{l(J)} \equiv \mathbf{h}\hat{\mathbf{s}}/N_\alpha$ , then the integral is evaluated exactly. The small length-scale assumption is consistent with the use of a low-order interpolation scheme to evaluate  $F_{Jlm}(\mathbf{r} - \mathbf{R}_{l(J)})$  on the discrete real-space grid defined by the trapezoidal rule integration when, as

is nearly always the case,  $\mathbf{R}_{l(j)}$  does not lie on the discrete real-space grid.

To derive an accurate, continuously differentiable interpolation formula, the large length-scale assumption is invoked to express the projector in a Fourier series, Equation (19):

$$F_{Jlm}(\mathbf{h}\mathbf{s} - \mathbf{R}_{l(j)}) = \frac{1}{V} \sum_{\mathbf{g}} \tilde{F}_{Jlm}(\mathbf{g}) e^{i\mathbf{g} \cdot (\mathbf{h}\mathbf{s} - \mathbf{R}_{l(j)})} \quad (19)$$

and to use the Fourier transform  $\tilde{F}_{Jlm}(\mathbf{g})$  given in Equation (8), in lieu of the Fourier series coefficients. Also, given the simulation cell is larger than  $r_{\text{cut}}$ , the reciprocal lattice vectors of the simulation cell can be employed to define the  $\mathbf{g}$ -space without loss of accuracy. (Note, the assumptions underlying Equation (19) form the basis for Equations (6)–(11), that is, the large length-scale approximation is always made.) The volume factors exactly cancel and will be neglected below. Next, the Euler exponential spline approximation to the atomic structure factor is introduced to yield the interpolation formula, Equation (20):

$$F_{Jlm}(\mathbf{h}\mathbf{s}' - \mathbf{R}_{l(j)}) \approx F_{l(j)Jlm}^{(\text{EES})}(\mathbf{h}\mathbf{s}' - \mathbf{R}_{l(j)}) \\ \equiv \sum_{\hat{\mathbf{s}}} \left[ \prod_{\alpha} M_p(u_{l(j),\alpha} + \hat{s}_{\alpha} - \hat{s}'_{\alpha}) \right] \chi_{Jlm}(\hat{\mathbf{s}}) \quad (20) \\ \chi_{Jlm}(\hat{\mathbf{s}}) = \sum_{\hat{\mathbf{g}}} \left[ \prod_{\alpha} e^{2\pi i \hat{g}_{\alpha} \hat{s}_{\alpha} / N_{\alpha}} d_p(\hat{g}_{\alpha}, N_{\alpha}) \right] \tilde{F}_{Jlm}(\hat{\mathbf{g}})$$

which possesses  $p-2$  continuous derivatives in the atomic coordinates. Note, the Fourier series is **not** truncated at  $2\hat{\mathbf{g}}_{\text{max}} = (N_{\alpha}N_bN_c)$  which indicates that the projector can vary on length scales smaller than  $s_{\alpha} = N_{\alpha}^{-1}$ . Letting  $\hat{\mathbf{g}} \rightarrow \hat{\mathbf{g}} + \hat{\mathbf{G}}$ , where  $-N_{\alpha}/2 < \hat{\mathbf{g}} \leq N_{\alpha}/2$  and  $\hat{\mathbf{G}} = M_{\alpha}N_{\alpha}$ , we have Equation (21):

$$\chi_{Jlm}(\hat{\mathbf{s}}) = \sum_{\hat{\mathbf{g}}} \left[ \sum_{\hat{\mathbf{G}}} \tilde{F}_{Jlm}(\hat{\mathbf{g}} + \hat{\mathbf{G}}) \right] \left[ \prod_{\alpha} e^{2\pi i \hat{g}_{\alpha} \hat{s}_{\alpha} / N_{\alpha}} d_p(\hat{g}_{\alpha}, N_{\alpha}) \right] \quad (21)$$

because  $d_p(\hat{g}_{\alpha}, N_{\alpha})$  and the complex exponentials are periodic functions of  $\hat{\mathbf{G}}$ . The functions,  $\tilde{F}_{Jlm}(\hat{\mathbf{g}} + \hat{\mathbf{G}})$ , go to zero exponentially quickly at large argument,  $|\hat{\mathbf{g}} + \hat{\mathbf{G}}|$  and convergence of the  $\hat{\mathbf{G}}$  sum is rapid. Thus, the  $\chi_{Jlm}(\hat{\mathbf{s}})$  can be evaluated, once, using a 3DFFT and stored for points in which  $|\mathbf{h}\mathbf{s}'| < r_{\text{cut}}$ . Note, it has been implicitly assumed that  $\exp(i\mathbf{g} \cdot \mathbf{R}_{l(j)})$  is a periodic function of  $\mathbf{G}$  which is not valid unless  $\mathbf{R}_{l(j)}$  is on a grid point. Introducing the sum over all  $\mathbf{G}$  ensures that the interpolation is exact when  $\mathbf{R}_{l(j)}$  lies on a grid point and forms a smoother function when  $\mathbf{R}_{l(j)}$  is not (e.g., a truncated Fourier series tends to oscillate at long range rather than smoothly approaching zero). Finally, it is convenient to take the parameters,  $N_a \times N_b \times N_c$  defining the discrete real space to be equal to those employed to create the electron density, as this permits the nonlocal computation to be interleaved with the computation of the electron density as well as ensuring accuracy, as describe above. This is in contrast to the NLEES-G technique, where the

flexibility of employing smaller  $N_a \times N_b \times N_c$  will be shown to give higher efficiency.

The gradient of the nonlocal energy with respect to the Fourier coefficients of the orbitals can be computed in a similar fashion. First, the gradient is expressed in the discrete real space, Equation (22):

$$\frac{dE_{\text{NL}}}{d\psi_i^*(\mathbf{r})} = \frac{f_i}{\prod_{\alpha} N_{\alpha}} \sum_J \sum_{l(j)} \sum_{lm} C_{Jl} F_{l(j)Jlm}^{(\text{EES})}(\mathbf{r} - \mathbf{R}_{l(j)}) Z_{il(j)Jlm} \quad (22)$$

as a loosely defined functional derivative and the corresponding gradient in  $\mathbf{g}$ -space obtained by performing a 3DFFT, Equation (23):

$$\frac{\partial E_{\text{NL}}}{\partial \psi_i^*(\mathbf{g})} = \frac{f_i}{\prod_{\alpha} N_{\alpha}} \sum_{\hat{\mathbf{s}}} e^{-i\mathbf{g} \cdot \mathbf{h}\mathbf{s}} \left[ \sum_J \sum_{l(j)} \sum_{lm} C_{Jl} F_{l(j)Jlm}^{(\text{EES})}(\mathbf{r} - \mathbf{R}_{l(j)}) Z_{il(j)Jlm} \right] \quad (23)$$

In practice, Equation (23) need not be evaluated explicitly. Rather, Equation (22) can be added to the action of the Kohn–Sham potential on the orbitals, and the total gradient subsequently back fast Fourier transformed into  $\mathbf{g}$ -space, thereby increasing efficiency.

The forces on the atoms can also be computed in a straightforward manner. As evident from Equations (20), (21), and (18), the only part of the nonlocal energy expression that depends on the atom position is the Cardinal B-spline,  $M_p(u_{l(j),\alpha} - \hat{s}_{\alpha})$ . Therefore, the derivative of  $E_{\text{NL}}$  with respect to the atom position can be computed easily using the fact that  $M_p(u)$  is continuously differentiable according to Equation (13). The resulting atomic forces are continuous and exact within the Euler exponential spline approximation to  $E_{\text{NL}}$ . Hence, the stability of a Car–Parrinello ab initio molecular dynamics calculation<sup>[4]</sup> is ensured, in contrast to previous methods.<sup>[16]</sup>

The NLEES-R procedure for the computation of the nonlocal pseudopotential energy, atomic force, and orbital gradient in real space can be summarized as follows:

1. Compute  $\tilde{F}_{Jlm}(\mathbf{g})$  using Equation (8) and multiply by the spline weight  $d_p(\mathbf{g}_{\alpha}, N_{\alpha})$ . The resulting functions are transformed to the discrete real space grid via a 3DFFT to create the  $\chi_{Jlm}(\hat{\mathbf{s}})$  which are stored on the desired range,  $|\mathbf{h}\mathbf{s}'| < r_{\text{cut}}$  for the duration of the simulation.
2. Multiply  $\chi_{Jlm}(\hat{\mathbf{s}})$  by the Cardinal B-spline,  $M_p(u_{l(j),\alpha} d + (-\hat{s}'_{\alpha} + \hat{s}_{\alpha}))$ , and sum over the discrete grid,  $\hat{s}_{\alpha}$  for each atom, Equation (21) for all points within the radial cutoff. This yields  $F_{l(j)Jlm}^{(\text{EES})}(\mathbf{h}\mathbf{s}' - \mathbf{R}_{l(j)})$  on the discrete grid with a slightly larger radial cutoff.
3. The calculation of force on the atoms, proceeds as in step (2), except that the derivative of Cardinal B-spline with respect to the atom position is employed in place of the Cardinal B-spline, itself. Steps (2) and (3) are the most computationally intensive.
4.  $Z_{il(j)Jlm}$  is computed using Equation (18). In practice, this step can be carried out along with the calculation of the real-space density  $n(\mathbf{r})$ , when the orbitals in real-space are avail-

able. The derivative of  $Z_{j(l)jm}$  with respect to the atom position can be obtained in the same way. The nonlocal energy and its contribution to the atom force are subsequently computed via Equation (5).

- The gradient with respect to the plane wave expansion coefficients of each orbital is computed in the real space as described in Equation (22) and added to the action of the KS potential on the orbitals. The sum is then transformed into  $\mathbf{g}$ -space by a 3DFFT.

The algorithmic procedure shown above makes it clear that, unlike the NLEES-G method, the computational overhead for NLEES-R does not depend on the number of nonlocal atom types. However, the memory requirement for NLEES-R exceeds that of NLEES-G, since the functions  $\chi_{jlm}(\mathbf{s})$  are stored on the full FFT grid for each nonlocal atom type in NLEES-R, while for NLEES-G,  $\tilde{F}_{jlm}(\mathbf{g})$  are stored on the small reciprocal-space grid for each atom type. Therefore, in choosing which method to apply, both the number of nonlocal atom types and the system size should be taken into account.

### 3. Results and Discussion

Solid silicon and liquid water have been selected to explore the applicability of the Euler exponential spline approach to the nonlocal energy and force calculations (NLEES) within a density functional theory framework. For silicon, a Bachelet–Hamann–Schluter type pseudopotential<sup>[27]</sup> was used to treat the core electrons in conjunction with the local density approximation (LDA). For water, the BLYP generalized gradient exchange–correlation (GGA) functional<sup>[28,29]</sup> with a Troullier–Martins type pseudopotential<sup>[30]</sup> was employed. The oxygen pseudopotential is quite hard and short ranged, whereas the silicon pseudopotential is soft and extends to a larger radial distance. Therefore, these contrasting systems allow the accuracy and efficiency of the new algorithms to be stringently tested. All calculations reported herein were performed using the PINY\_MD package,<sup>[31]</sup> in which the new approaches were implemented.

To investigate the accuracy of the NLEES method, the nonlocal energy of water and silicon dimer systems obtained from the standard plane wave method and the NLEES approaches are compared. For silicon, a dimer with an internuclear distance  $r=1.88 \text{ \AA}$  was placed in a cubic box of length  $L=8 \text{ \AA}$

while for water, a dimer was placed in a cubic box of  $L=10 \text{ \AA}$ . In both systems, the  $\mathbf{g}$ -space based approach of Martyna and Tuckerman<sup>[8]</sup> was employed for treating the cluster boundary conditions. Additionally, a rather large simulation cell was employed in order to test the convergence of NLEES-R with respect to radial cutoff,  $r_{\text{cut}}$ .

The results for the dimer systems are summarized in Tables 1 and 2 for the NLEES-G and the NLEES-R methods, respectively. It is evident from Table 1 that NLEES-G, with a spline interpola-

**Table 1.** Nonlocal energy of silicon and water dimers expressed in Hartree, obtained from the standard plane wave method (PW) and the NLEES-G technique. The quantities  $\Delta(p=8)$  and  $\Delta(p=6)$  are the deviation of the NLEES-G energy from the exact PW result expressed in micro-Hartree ( $\mu\text{Ha}$ ) using an interpolation order of  $p=8$  and  $p=6$ , respectively. An FFT grid of side  $2 \times N^{(\text{orb})} = N^{(\text{dens})}$  was employed throughout.

$\text{Si}_2$					
$E_{\text{cut}}$ [Ry]	PW	NLEES-G( $p=8$ )	$\Delta(p=8)$	NLEES-G( $p=6$ )	$\Delta(p=6)$
15	0.2499081	0.2499088	0.7	0.2499231	15
20	0.2485220	0.2485221	0.1	0.2485262	4.2
25	0.2483740	0.2483741	0.1	0.2483782	4.2
$(\text{H}_2\text{O})_2$					
$E_{\text{cut}}$ [Ry]	PW	NLEES-G( $p=8$ )	$\Delta(p=8)$	NLEES-G( $p=6$ )	$\Delta(p=6)$
70	3.5948133	3.5948141	0.8	3.5948348	21.5

**Table 2.** The nonlocal energy of silicon and water dimers obtained from the real-space method, NLEES-R, as a function of spherical cutoff radius,  $r_{\text{cut}}$ . The results with no spherical truncation are nearly identical to those of NLEES-G. The numbers in square brackets are the deviations of the NLEES-R energy from the exact (PW) result expressed in  $\mu\text{Ha}$ .

$r_{\text{cut}}$ [bohr]	$\text{Si}_2$			$(\text{H}_2\text{O})_2$
	15 Ry	20 Ry	25 Ry	70 Ry
2.5				3.5947951[−18.2]
3.5	0.2497878[−120.3]	0.2485481[26.1]	0.2484007[26.7]	3.5948146[1.3]
4.5	0.2499081[0]	0.2485197[−2.3]	0.2483718[−2.2]	3.5948138[0.5]
5.5	0.2499137[5.6]	0.2485232[1.2]	0.2483751[1.1]	3.5948147[1.4]
7.5	0.2499086[0.5]	0.2485222[0.2]	0.2483741[0.1]	3.5948140[0.7]

tion order  $p=8$ , leads to excellent agreement with the standard plane-wave calculation for both silicon and water systems. The agreement is better than  $\Delta E \approx 10^{-6} \text{ Ha} \approx 0.3 \text{ K}$ , with a typical  $E_{\text{cut}}=15 \text{ Ry}$  plane wave cutoff for silicon and  $E_{\text{cut}}=70 \text{ Ry}$  cutoff for water. As shown in Table 1, the accuracy improves as the energy cutoff for silicon is increased. For NLEES-R, the accuracy and the CPU time depend on the spherical truncation radius,  $r_{\text{cut}}$ . As shown in Table 2, NLEES-R works well for the water dimer, with an interpolation order of  $p=8$  and a radial cutoff  $r_{\text{cut}}=3.5 \text{ bohr}$ . In silicon, the cutoff radius must be taken to be larger in order to obtain acceptable accuracy, owing to the longer range of the pseudopotential. Using  $r_{\text{cut}}=4.5 \text{ bohr}$ , the accuracy obtained for the nonlocal energy of the silicon dimer is  $\Delta E \approx 10^{-6} \text{ Ha}$ .

To demonstrate the improved scaling of the new methods with system size, a series of solid silicon and liquid water systems were studied using NLEES-G, NLEES-R and the standard plane-wave technique at the  $\Gamma$  point. The total energy of sili-

**Table 3.** The nonlocal energy per atom of solid silicon obtained from the standard plane wave technique (PW) and the NLEES-G method with a spline order  $p=8$  for system sizes to  $N=192$  silicon atoms, are presented. The quantities  $\Delta$  are the deviations from the exact result expressed in  $\mu\text{Ha}$ . An FFT grid of side  $2 \times N^{(\text{orb})} = N^{(\text{dens})}$  was employed throughout.

No. of Si	PW	NLEES-G	$\Delta$
8	0.08435194	0.08435194	0
16	0.09272945	0.09272948	0.03
32	0.09590086	0.09590091	0.05
48	0.09711667	0.09711676	0.09
64	0.09453666	0.09453673	0.07
96	0.09629711	0.09629723	0.12
128	0.09609518	0.09609536	0.18
144	0.09692763	0.09692779	0.16
192	0.09701243	0.09701266	0.23

con in the diamond lattice for lattices containing up to  $N=192$  atoms was investigated using an  $E_{\text{cut}}=15$  Ry plane-wave cutoff. Results are presented in Table 3 for NLEES-G and the standard plane-wave method. The nonlocal energies generated by the NLEES-G method are in good agreement with those generated by the exact standard method. The relative accuracy of NLEES-G does not decrease as the system size increases. Figure 1a shows the total CPU time needed to compute the nonlocal energy and forces for the silicon systems using the standard plane-wave method and the NLEES-G method. The solid lines are fits of the data to the respective scaling law of the corresponding technique. For the standard plane-wave calculation, the CPU time follows the predicted  $N^3$  scaling law almost perfectly. On the basis of the analysis in the previous section, the NLEES-G method should possess an  $NM \log M = N^2 \log N$  scaling law, since  $M \propto N$ . However, there is little difference between an  $N^2 \log N$  and an  $N^2$  scaling law for the two decades of system size tested. In fact, the fit shown in Figure 1a for the NLEES-G method predicts  $N^2$  scaling. As evident from Figure 1, the NLEES-G method at an accuracy of  $\Delta E \approx 10^{-6}$  Ha becomes more computationally efficient than the standard technique for systems containing approximately or more than 16 atoms. This represents an order-of-magnitude improvement over the exact  $N^2 \log N$  approaches introduced previously.<sup>[17, 18]</sup>

A similar analysis of liquid water with system sizes ranging from  $N_{\text{mol}}=8$  to  $N_{\text{mol}}=112$  molecules at a density of  $\rho=1$  g cm<sup>-3</sup> has been performed using a plane-wave cutoff of  $E_{\text{cut}}=70$  Ry. In Table 4, the nonlocal energies obtained from the standard plane-wave method, the NLEES-G method, and the NLEES-R method with  $r_{\text{cut}}=3.5$  bohr and  $r_{\text{cut}}=3.0$  bohr, are reported. The accuracy of the NLEES-R method with  $r_{\text{cut}}=3.5$  bohr is comparable to that of the NLEES-G method regardless of system size. Using a smaller radial cutoff,  $r_{\text{cut}}=$

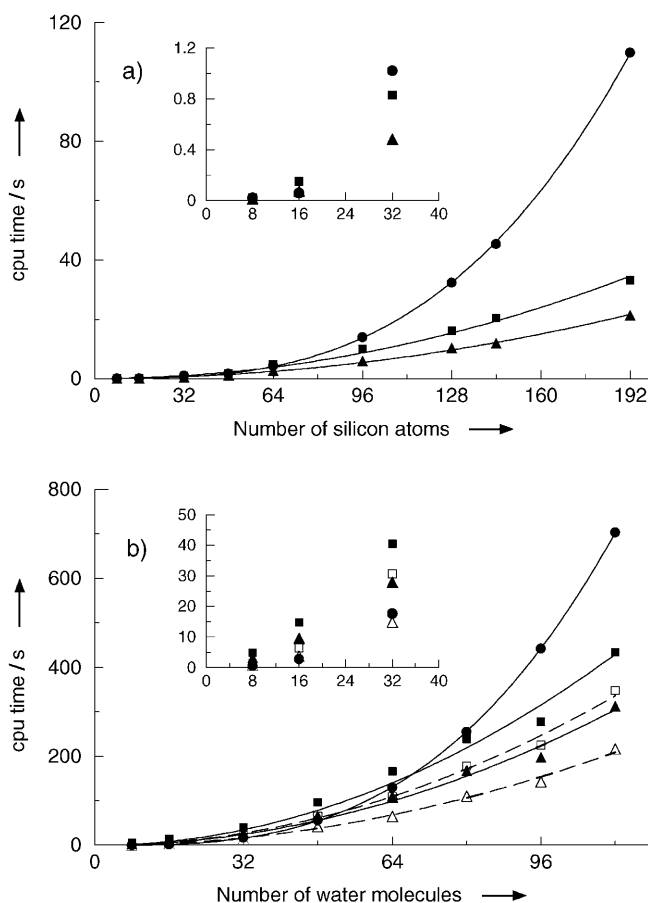


**Figure 1.** a) The CPU time required to compute the nonlocal energy and force using the standard method (●) and the NLEES-G method with  $p=8$  for silicon in the diamond structure. Results for FFT grids of side  $2 \times N^{(\text{orb})} = N^{(\text{dens})}$  (■) and  $1.6 \times N^{(\text{orb})}$  (▲) are depicted. b) The CPU time of the standard plane-wave calculation (●), NLEES-R with  $r_{\text{cut}}=3.5$  bohr (■) and with  $r_{\text{cut}}=3.0$  bohr (▲) for the water system at density of  $\rho=1.0$  g cm<sup>-3</sup>. NLEES-G results using FFT grids of side  $2 \times N^{(\text{orb})}$  with  $p=8$  (□) and  $1.5 \times N^{(\text{orb})}$  with  $p=12$  (△) are, also, shown. Solid lines (—) are fits to the data using the  $N^3$  scaling law for the standard method and the  $N^2$  scaling law for the NLEES-R. Dashed lines (---) are fits to the NLEES-G method using an  $N^2$  scaling law.

**Table 4.** The nonlocal energy of liquid water at a density of  $\rho=1.0$  g cm<sup>-3</sup> obtained from the standard plane wave (PW), NLEES-G, and NLEES-R methods is compared for systems up to  $N_{\text{mol}}=112$  water molecules. The reported energy is the nonlocal energy per single water molecule. The number in square brackets is the deviation from the exact result of the standard method in  $\mu\text{Ha}$  at a given system size. An FFT grid of side  $2 \times N^{(\text{orb})} = N^{(\text{dens})}$  was employed throughout.

No. of H <sub>2</sub> O	PW	NLEES-G	NLEES-R(3.5 <sup>[a]</sup> )	NLEES-R(3.0 <sup>[a]</sup> )
8	1.7857781	1.7857783[0.2]	1.7857780[-0.1]	1.7857816[3.5]
16	1.8249863	1.8249866[0.3]	1.8249865[0.2]	1.8249894[3.1]
32	1.7772500	1.7772503[0.3]	1.7772503[0.3]	1.7772526[2.6]
48	1.7882401	1.7882403[0.2]	1.7882396[-0.5]	1.7882417[1.6]
64	1.8094158	1.8094161[0.3]	1.8094156[-0.2]	1.8094184[2.6]
80	1.7969129	1.7969130[0.1]	1.7969128[-0.1]	1.7969137[0.8]
96	1.8149476	1.8149479[0.3]	1.8149479[0.3]	1.8149497[2.1]
112	1.8150260	1.8150262[0.2]	1.8150258[-0.2]	1.8150272[1.2]

[a] Cutoff radii in Bohr.

3.0 bohr, yields slightly lower accuracy, but reduces the CPU time substantially. Figure 1b shows the CPU time required to compute the nonlocal energy and forces for the water systems of Table 4 at an accuracy level of  $\Delta E \approx 10^{-6}$  Ha for  $N_{\text{mol}} = 32$  water molecules. The solid lines are fits of the data to the predicted scaling law,  $N^3$  for the standard method and  $N^2$  for both the NLEES-R and NLEES-G methods. It is clear from Figure 1 that the NLEES-G method performs better than NLEES-R for liquid water. NLEES-G becomes more computationally efficient than the standard method for systems containing approximately 24 or more water molecules, which means 24 nonlocal atoms since hydrogen atoms are treated with a local pseudopotential. NLEES-R with  $r_{\text{cut}} = 3.0$  bohr becomes more efficient when approximately 48 water molecules or more are present. However, we note that the efficiency of the NLEES-G method depends on the number of nonlocal atom types and the cross-over point will be pushed further out if there is more than one nonlocal atom type in the system.

Although the nonlocal energy of the NLEES methods is not exact, it possesses many continuous derivatives, in contrast to other methods,<sup>[16]</sup> and, as demonstrated above, can be tuned to yield very high accuracy without loss of efficiency. This makes the NLEES technique ideal for use in Car–Parrinello<sup>[4]</sup> ab initio molecular dynamics simulation studies (CPAIMD). In order to demonstrate the stability of the NLEES-R approach, a CPAIMD simulation of  $N_{\text{mol}} = 8$  water molecules was performed. The simulation was carried out with a plane wave cutoff of  $E_{\text{cut}} = 70$  Ry and a fictitious mass  $\mu = 400$  au in conjunction with a time step  $\Delta t = 0.075$  fs. The  $N_{\text{mol}} = 8$  water molecules were placed in a cubic periodic box of length  $L = 6.208$  Å and annealed to a temperature of  $T = 300$  K. Next, a canonical ensemble (NVT) simulation was carried out for  $t = 2$  ps at  $T = 300$  K using the Nose–Hoover chain canonical dynamics technique.<sup>[32]</sup> In Figure 2, the temperature of electronic degrees of freedom and the average magnitude of the fictitious force acting on plane wave coefficients as a function of simulation time using the NLEES-R form of the nonlocal energy and force with  $r_{\text{cut}} = 3.0$  bohr, are shown. If the simulation had become unstable or there were a noticeable exchange of energy between atomic and electronic degrees of freedom, both quantities shown in Figure 2 would have sharply increased during the simulation. As Figure 2 indicates, the NLEES-R method generates a stable trajectory. Similar results have been generated using NLEES-G (not shown).

#### 4. Conclusions

Two new approaches based on Euler exponential spline interpolation have been developed to evaluate the electron–atom nonlocal pseudopotential interaction. Both reciprocal-space, NLEES-G, and real-space, NLEES-R, based techniques were derived and shown to improve the scaling with system size of the nonlocal energy and force calculations without sacrificing accuracy. The *g*-space-based method was shown to scale as  $NM \log M \sim N^2 \log N$ , while the real-space-based method was shown to scale as  $NM \sim N^2$ . The NLEES methods became more efficient than standard methods very quickly, at around 20

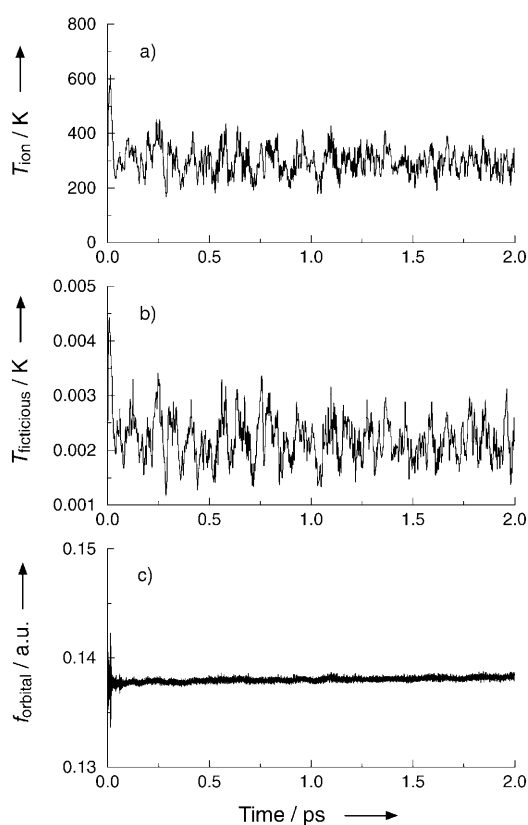


**Figure 2.** a) The instantaneous ion temperature, b) the instantaneous temperature of fictitious electronic degrees of freedom, and c) the average forces acting on orbital coefficients, obtained from a CPAIMD simulation of an  $N_{\text{mol}} = 8$  water system at  $T = 300$  K. The simulation was performed using the NLEES-R method for the nonlocal part of the energy and force calculation with  $r_{\text{cut}} = 3.0$  bohr.

nonlocal atoms or more for the systems considered herein. It was also demonstrated that ab initio molecular dynamics calculations within the Car–Parrinello framework can be performed without any loss of stability or adiabaticity using NLEES methods, owing to the continuous derivatives provided by the exponential spline.

Before closing, we briefly discuss the possibility of achieving  $\mathcal{O}(N)$  scaling for the nonlocal energy and force calculation. In the NLEES-R method, the calculation of  $Z_{i(j)jlm}$  in Equation (18) must be performed for each state and each ion to obtain the nonlocal energy through Equation (5), which leads to the  $\mathcal{O}(N^2)$  scaling. However, if each orbital can be localized in the region of an ion by exploiting the unitary invariance of the total energy, then the sums over states and ions can be restricted to a single sum over ions and their “associated” states, hence leading to linear scaling with system size. However, these orbitals, known as Wannier orbitals, are not preserved in the Car–Parrinello calculation. Recently, Tuckerman and co-workers<sup>[13,14]</sup> showed that the Car–Parrinello Lagrangian could be reformulated in a gauge-invariant manner so that the resulting Car–Parrinello type equations automatically preserve the Wannier orbitals as the system evolves. Thus, by combining the current NLEES-R method with the dynamical orbital localization scheme, we expect to achieve overall  $\mathcal{O}(N)$  scaling for Car–Par-

rinello molecular dynamics calculations. In a similar manner, by combining the reciprocal-space localization functional of Iannuzzi and Parrinello<sup>[12]</sup> with the aforementioned gauge-fixing approach,<sup>[13,14]</sup> it should be possible to achieve  $\mathcal{O}(N \ln N)$  scaling with the NLEES-G method. Investigation of such possibilities constitutes ongoing and future work.

## Acknowledgements

The authors gratefully acknowledge Dawn A. Yarne for helpful discussions. This work was supported by NSF CHE-0121375 and NSF CHE-0310107 (HSL and MET) and IBM Research and NSF-0229959 (GJM).

**Keywords:** ab initio calculations · molecular dynamics · silicon · splines · water

- [1] M. Parrinello, *Solid State Commun.* **1997**, *102*, 107.  
 [2] D. Marx, J. Hutter in *Modern Methods and Algorithms of Quantum Chemistry, NIC Series, Vol. 1* (Ed.: J. Grotendorst), Forschungszentrum, Juelich, **2000**.  
 [3] M. E. Tuckerman, *J. Phys.: Condens. Matter* **2002**, *14*, R1297.  
 [4] R. Car, M. Parrinello, *Phys. Rev. Lett.* **1985**, *55*, 2471.  
 [5] C. K. Chu, *An Introduction to Wavelets*, Academic Press, Boston, MA, **1992**.  
 [6] I. J. Schoenberg, *Cardinal Spline Interpolation*, Society for Industrial and Applied Math, Philadelphia, PA, **1973**.  
 [7] U. Essmann, L. Perrera, M. L. Berkowitz, T. Darden, H. Lee, L. G. Pedersen, *J. Chem. Phys.* **1995**, *103*, 8577.  
 [8] G. J. Martyna, M. E. Tuckerman, *J. Chem. Phys.* **1999**, *110*, 2810.  
 [9] P. Minary, J. Morrone, D. Yarne, M. E. Tuckerman, G. J. Martyna, *J. Chem. Phys.* **2004**, *121*, 11 949.  
 [10] P. Minary, M. E. Tuckerman, K. A. Pihakari, G. J. Martyna, *J. Chem. Phys.* **2002**, *116*, 5351.  
 [11] A. Toukmajo, C. Sagui, J. Board, T. Darden, *J. Chem. Phys.* **2000**, *113*, 10913.  
 [12] M. Iannuzzi, M. Parrinello, *Phys. Rev. B* **2002**, *66*, 1552209.  
 [13] R. Iftimie, J. W. Thomas, M. E. Tuckerman, *J. Chem. Phys.* **2004**, *120*, 2169.  
 [14] J. W. Thomas, R. Iftimie, M. E. Tuckerman, *Phys. Rev. B* **2004**, *69*, 125105.  
 [15] A. N. Nicholson, R. L. Hayes, M. E. Tuckerman, unpublished results.  
 [16] R. D. King-Smith, M. C. Payne, J. S. Lin, *Phys. Rev. B* **1991**, *44*, 13 063.  
 [17] S. Goedecker, *Philos. Mag. A* **1994**, *70*, 305.  
 [18] S. P. Lewis, C. Y. Wei, E. J. Mele, A. M. Rappe, *Phys. Rev. B* **1998**, *58*, 482.  
 [19] L. Kleinman, D. M. Bylander, *Phys. Rev. Lett.* **1982**, *48*, 1425.  
 [20] D. Vanderbilt, *Phys. Rev. B* **1990**, *41*, 7892.  
 [21] S. Goedecker, M. Teter, J. Hutter, *Phys. Rev. B* **1996**, *54*, 1703.  
 [22] C. Hartwigsen, S. Goedecker, J. Hutter, *Phys. Rev. B* **1998**, *58*, 3641.  
 [23] G. Lippert, J. Hutter, M. Parrinello, *Mol. Phys.* **1997**, *92*, 477.  
 [24] Y. Liu, D. A. Yarne, M. E. Tuckerman, *Phys. Rev. B* **2003**, *68*, 125 110.  
 [25] K. Varga, Z. Y. Zhang, S. T. Pantelides, *Phys. Rev. Lett.* **2004**, *93*, 176403.  
 [26] X. Gonze, P. Kackell, M. Scheffler, *Phys. Rev. B* **1990**, *41*, 12 264.  
 [27] G. B. Bachelet, D. R. Hamann, M. Schluter, *Phys. Rev. B* **1982**, *26*, 4199.  
 [28] A. D. Becke, *Phys. Rev. A* **1988**, *38*, 3098.  
 [29] C. Lee, W. Yang, R. C. Parr, *Phys. Rev. B* **1988**, *37*, 785.  
 [30] N. Troullier, J. L. Martins, *Phys. Rev. B* **1991**, *43*, 1993.  
 [31] M. E. Tuckerman, D. A. Yarne, S. O. Samuelson, A. L. Hughes, G. J. Martyna, *Comput. Phys. Commun.* **2000**, *128*, 333.  
 [32] G. J. Martyna, M. L. Klein, M. Tuckerman, *J. Chem. Phys.* **1992**, *97*, 2635.

Received: March 2, 2005